

RESEARCH ARTICLE

MicroCT-Based Virtual Histology Evaluation of Preclinical Medulloblastoma

Suresh I. Prajapati,¹ Aoife Kilcoyne,^{1,2} Aislynn K. Samano,¹ Dustin P. Green,¹ Steven D. McCarthy,¹ Barron A. Blackman,¹ Michelle M. Brady,¹ Lee Ann Zarzabal,³ Arun K. Tatiparthi,⁴ Timothy J. Sledz,⁴ Timothy Duong,⁵ Sachiko Ohshima-Hosoyama,¹ Francis J. Giles,² Joel E. Michalek,³ Brian P. Rubin,⁶ Charles Keller^{1,7,8}

¹Greehey Children's Cancer Research Institute, University of Texas Health Science Center, 8403 Floyd Curl Drive, MC-7784 San Antonio, TX 78229, USA

²Department of Medicine, University of Texas Health Science Center, 7703 Floyd Curl, San Antonio, TX 78229, USA

³Epidemiology and Biostatistics, University of Texas Health Science Center, 7703 Floyd Curl, San Antonio, TX 78229, USA

⁴Microphotonics Inc., Allentown, PA, USA

⁵Research Imaging Institute, University of Texas Health Science Center, 7703 Floyd Curl, San Antonio, TX 78229, USA

⁶Department of Anatomic Pathology, Cleveland Clinic, Taussig Cancer Center and the Lerner Research Institute, Cleveland, OH, USA

⁷Cellular and Structural Biology, University of Texas Health Science Center, 7703 Floyd Curl, San Antonio, TX 78229, USA

⁸Pediatrics University of Texas Health Science Center, 7703 Floyd Curl, San Antonio, TX 78229, USA

Abstract

Purpose: The purpose of this paper is to validate a rapid and cost-effective *ex vivo* technique, microCT-based virtual histology, as an alternative to MRI imaging for assessing the therapeutic response in genetically engineered mouse models of cancer.

Procedures: All animal procedures were conducted in accordance with the Guidelines for the Care and Use of Laboratory Animals and were approved by the Institutional Animal Care and Use Committee (IACUC) at the University of Texas Health Science Center at San Antonio. MRI imaging was performed on 6-week-old, bortezomib-treated genetically engineered *Patched1*, *p53* mice that recapitulate the characteristics of human medulloblastoma. After MRI scans, the same mice were euthanized to collect brain or spine samples for virtual histology staining followed by microCT scanning.

Results: Nine-micrometer resolution *ex vivo* micro X-ray computed tomography (microCT)-based virtual histology images were qualitatively reflective of high-field live animal images obtained with magnetic resonance imaging (MRI) and histopathology. Cerebellar volumes on microCT-based virtual histology correlated closely with MRI cerebellar volumes ($R=0.998$). MRI and microCT-based virtual histology both indicated a significant difference between cerebellar volumes of untreated and treated mice ($p=0.02$ and $p=0.04$, respectively). The *ex vivo* microCT method also allowed a 7,430-fold improvement in voxel resolution (voxel volume of $729 \mu\text{m}^3$ for $9\text{-}\mu\text{m}$ isometric resolution microCT vs. $5,416,800 \mu\text{m}^3$ for $400\times 111\times 122 \mu\text{m}$ resolution MRI) at a 28% cost savings (\$400 vs. \$555 per animal).

Significance: MicroCT-based virtual histology represents a versatile quantitative imaging method for anatomical imaging of the neuro-axis in preclinical models.

Electronic supplementary material The online version of this article (doi:10.1007/s11307-010-0372-3) contains supplementary material, which is available to authorized users.

Correspondence to: Charles Keller; e-mail: keller@ohsu.edu

Conclusion: The *ex vivo*, en bloc technique of microCT-based virtual histology matched MRI in reflecting histopathology. MicroCT-based virtual histology proved to be a more cost-effective technique and less labor-intensive. On the other hand, MRI provides ability to perform *in vivo* imaging, faster scanning and lower radiation dose by sacrificing the spatial resolution. Thus, both *in vivo* MRI and *ex vivo* microCT-based virtual histology are effective means of quantitatively evaluating therapeutic response in preclinical models of cerebellar tumors including the childhood cancer, medulloblastoma.

Key words: Medulloblastoma, Imaging, MRI, MicroCT, Virtual histology, Therapeutics

Introduction

Medulloblastoma is the most common pediatric central nervous system malignancy and the most common primary tumor of the posterior fossa in children [1]. Medulloblastomas arise in either the vermis or the lateral cerebellar hemispheres [2] from neuronal stem cells in these locations. Clinically, medulloblastoma is one of the most aggressive malignant brain tumors of childhood, a disease for which new molecular-targeted strategies are needed.

Magnetic resonance imaging (MRI) is the clinical gold standard for assessment of brain tumors at diagnosis and during therapy. Compared with X-ray computed tomography (CT), MRI provides more detailed images of parenchymal lesions, and is more sensitive in detecting lesions within the posterior fossa, subarachnoid spaces, and leptomeninges. Spine MRI is also the imaging modality of choice in staging tumors that have a predilection for leptomeningeal spread, such as medulloblastoma.

For preclinical therapeutic studies, we have developed a genetically engineered mouse model (GEMM) of medulloblastoma [3]. In recent studies, we have demonstrated the utility of live animal, high-field (7 T) MRI in assessing response to therapy in this model [4]. As a possible higher-resolution alternative, we present the validation of *ex vivo* microCT-based virtual histology (VH). MicroCT-based VH of soft tissue is a novel, rapid and inexpensive, non-destructive method for en bloc imaging at resolutions up to 1 μm [5, 6]. Furthermore, microCT-based VH specimens after scanning are also amenable to processing for traditional microtome sectioning and histopathology. In this study, we have explored the feasibility of microCT-based VH as an alternative to high-field MRI imaging for assessing tumor volume calculations and therapeutic response in a GEMM.

Materials and Methods

All animal procedures were conducted in accordance with the Guidelines for the Care and Use of Laboratory Animals and were approved by the Institutional Animal Care and Use Committee (IACUC) at the University of Texas Health Science Center at San Antonio.

Mice and Genotyping

Medulloblastoma-prone (MB) mice were generated and genotyped as previously described [6]. MB mice genotypes were *Ptc1*^{F1-2m/WT} *Trp53*^{F2-10/F2-10} *Pax7*^{1CNm/WT}. Control mice genotypes were *Ptc1*^{WT/WT} *Trp53*^{F2-10/F2-10} *Pax7*^{WT/WT}. The F2-10 allele for *Trp53* is functionally normal when the *Pax7*-Cre allele (*Pax7*^{1CNm}) is absent [3].

Therapeutic Administration

Bortezomib (Velcade™, hereafter abbreviated as VLCD) treatment (1 mg/kg) was administered to MB mice on postnatal day 21 (P21) by intraperitoneal injection once a week for 3 weeks. VLCD was suspended in dimethyl sulfoxide (DMSO) and was administered to MB mice undergoing treatment, whereas DMSO alone was used as the vehicle control treatment for MB mice and WT mice. The mice were divided into three groups, MB treated (MB-VLCD; $n=4$), MB non-treated (MB-DMSO; $n=4$), and WT non-treated (WT-DMSO; $n=2$). Mice were euthanized on P43, after *in vivo* MRI scans.

Magnetic Resonance Imaging

T2-weighted MRI scans were performed on a 7-T Bruker Biospec horizontal bore scanner (70/30USR; Bruker, Ettlingen, Germany) with a S057 gradient insert that can produce maximal gradient amplitude of 400 T/m. A custom-designed 10-mm-inner-diameter circular radiofrequency (RF) trans-receiver surface coil was used for signal acquisition. After performing the tri-pilot scan, multi-slice, contiguous sagittal images were captured with a rapid acquisition and relaxation enhancement (RARE) sequence with the following parameters: TE/TR=60/2571.22 ms, where TE is the echo times and TR is the repetition time; RARE factor=8; slice thickness=400 μm , slice step (gap) 500 μm , field of view (FOV)=15.6 \times 15.6 mm²; a matrix size of 140 \times 128 (in-plane resolution of 111 \times 122 μm ; voxel volume 5,416,800 μm^3), number of slices=20; image averages=16. Because the TR needs to be several seconds long to produce T2 weighting, a multi-slice sequence with contiguous slices was used instead of a 3D sequence to reduce the imaging time. Average scan time was 15 min.

Virtual Histology

After MRI scans, mice were euthanized, perfused with phosphate-buffered saline (PBS) and then 10% buffered formalin prior to

collecting brains for VH staining. Mice heads were denuded then removed from the body by scalpel incision below C2. The cranium was split starting at the nasal bone longitudinally to the occiput using narrow surgical scissor. Next, the posterior skull plates were removed using forceps to expose lateral hemispheres. The exposed brain, still in cranium base, was then placed in a 50-mL conical tube with 10% buffered formalin and rocked for 24 h at room temperature. After 24 h, a tiny slit approximately 1 mm in length was made using a # 11 scalpel in each of the lateral hemispheres for improved stain penetration. After fixing, the samples were transferred and washed in 5% sucrose–0.1 M phosphate buffer (pH 7.4) solution for 15 min, four times. Samples were then rinsed in PBS three times, rocking for 1 h each time at room temperature. After rinsing, the samples were stained overnight with a pre-commercial staining solution (Numira Biosciences, Salt Lake City, UT) at room temperature. The next day, the samples were rinsed with PBS three times while rocking at room temperature; once overnight and 1 h each time for another two washes.

MicroCT Imaging

MicroCT scans were performed on Skyscan1172 microCT system, with a cooled 12-bit 11-Mp camera and 10-W X-ray source (20–100 keV and 100–250 μ A). The brain samples were taken out of the PBS solution and then wrapped with parafilm to keep them moist during the scan. These samples were then mounted vertically onto the flat base specimen holder and scanned at 9 μ m voxel diameter (voxel volume of 729 μ m³), with the X-ray tube settings of 100 keV and 100 μ A with a 0.5-mm Al filter. The samples were rotated through 180° with an incremental rotation step of 0.40°. Twelve two-dimensional transmission images were acquired at each rotation step and averaged to increase the signal to noise ratio. The two-dimensional transmission projections were then reconstructed into trans-axial images along the longitudinal axis using the Feldkamp three-dimensional cone-beam reconstruction algorithm. Average scan time was 3 h.

Histopathology

After scanning, the VH-stained brains were paraffin-embedded, sectioned and examined histologically using hematoxylin and eosin (H&E) stains. Because the MRI data was acquired in sagittal slices, the brains were cut in to thin sagittal sections (3 μ m) in the plane that corresponded to MRI images.

Image Segmentations

To determine the effect of drug treatment on MB mice, the cerebellar volumes from MB-VLCD, MB-DMSO, and WT-DMSO mice brains were calculated from both MRI and CT imaging modalities by a single observer. Cerebellar volumes from MRI images were calculated on a slice by slice basis. The slice volumes were then combined for a total volume value. Cerebellar segmentations and volume calculation from microCT-based VH data were performed on Seg 3, an open-source software from the University of Utah Scientific Computing Institute (<http://www.sci.utah.edu/cibc/software>). Segmentations were done manually using a paint brush tool to highlight the cerebellum.

Treatment with VLCD In Vitro

Murine medulloblastoma primary cell cultures (UID 26137) were plated in 60 mm dish at 1×10^5 cells per dish and cultured overnight. The cells were treated at the indicated concentrations of VLCD (Velcade®, Millennium Pharmaceutical, Cambridge, MA) in 0.05% DMSO and harvested 24 h post treatment for western blot analysis.

Western Blot

Whole cell lysates were prepared from cells lysed following 24-h treatment with VLCD in RIPA and 100× HALT protease inhibitor (Thermo Scientific, Waltham, MA). Protein concentration was determined using the Lowry method. An aliquot of lysate was homogenized with loading buffer and heated at 95°C for 5 min. Protein samples, 20 μ g per lane, were electrophoresed on a 15% SDS-PAGE and transferred to a PVDF membrane (Fischer Scientific, Waltham, MA). Target proteins were detected using primary antibodies for Caspase-3 (anti-rabbit IgG 1:1,000 dilution, Cell Signaling Technology, Beverly, MA) and PCNA (anti-mouse IgG 1:1,000 dilution, Santa Cruz Biotechnology, Santa Cruz, CA). To control for protein loading, primary antibodies for β -actin were used (anti-rabbit IgG at 1:500,000, Sigma-Aldrich, St. Louis, MO). The blots were incubated with primary antibody overnight at 4°C and washed with 1× Tris-buffered saline Tween-20 (TBST) then incubated respectively with peroxidase-conjugated secondary antibody (anti-mouse or anti-rabbit IgG 1:5000, Vector Labs, Burlingame, CA) for 1 h and washed with 1× TBST. Chemiluminescence was detected using Super Signal West Pico or Dura (Pierce Protein Products, Rockford, IL).

Statistical Analysis

Brain volume comparisons by treatment (treated, untreated) and by measurement type (MRI, VH) were carried out with the exact Wilcoxon test. All statistical testing was two-sided with a significance level of 5%. SAS Version 9.1.3 for Windows (SAS Institute, Cary, North Carolina) was used for all statistical tests.

Results

MicroCT-based Virtual Histology is a High-resolution Ex Vivo Alternative to MRI

Representative images from microCT-based VH and MRI scans are shown in Fig. 1a, b. Mice from all three groups MB-VLCD, MB-DMSO, and WT-DMSO were imaged under anesthesia by T2-weighted MRI at postnatal day 43 (P43). The MRI data, being non-isotropic, had highest resolution in the sagittal plane (Fig. 1b). Upon completion of MRI scans, the mice were euthanized to collect their brains for microCT-based VH. The microCT data being isotropic, the resolution was uniform in all three anatomical planes (9 μ m; Fig. 1a). For these scanning parameters of comparable cost (\$400 for microCT-based virtual VH staining and scanning versus \$555 for MRI scans and anesthesia), a substantial

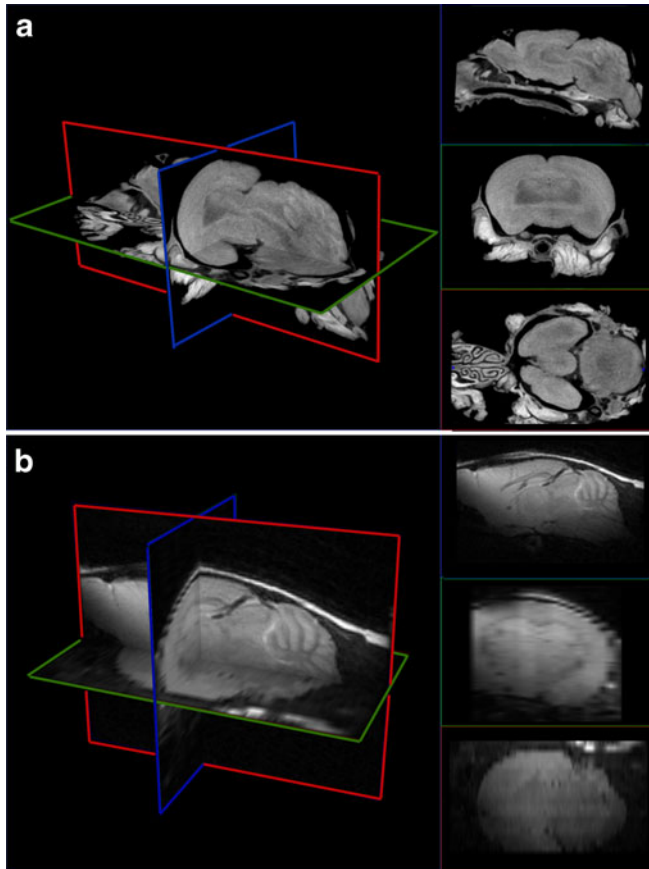


Fig. 1. Gross comparison between MRI and microCT-based VH scans. **a** microCT-based VH data scan showing all three anatomical planes for a wild type control mouse brain (9 μm isotropic resolution). **b** MRI scan showing all three anatomical planes for a wild type control mouse brain (111 $\mu\text{m} \times 122 \mu\text{m} \times 400 \mu\text{m}$).

7,430-fold improvement in voxel resolution was achieved with the *ex vivo* microCT method (voxel volume of 729 μm^3 for 9 μm isometric resolution microCT vs. 5,416,800 μm^3 for 400 \times 111 \times 122 μm resolution MRI).

MicroCT-based VH Accurately Demonstrates Histopathology Seen with MRI and Histology Images

After microCT scanning, samples were processed for traditional histopathology. Figure 2 shows representative images of WT-DMSO (Fig. 2a), MB-VLCD (Fig. 2b), and MB-DMSO (Fig. 2c) mice using MRI, microCT-based VH and H&E histology (from left to right). The MB-VLCD mouse brain images showed enlarged cerebella with folia layer thickening (Fig. 2b, pointed by arrowhead) whereas the MB-DMSO mouse brains showed large tumor masses (Fig. 2c, denoted by asterisk). The histology of MB-VLCD and MB-DMSO tumors were comparable and without evidence of overt treatment effect (Fig. 2d, e), which could in part be attributed to VLCD not being able to cross the blood-brain

barrier [7] unless disrupted by a tumor of sufficient size. Nevertheless, mitotic counts were significantly lower in treated than non-treated tumor cells that remained (4 vs. 31 per 10 HPF). To affirm that VLCD had an effect on survival, immunohistochemistry could not be satisfactorily performed on sectioned samples that had previously been stained for VH scans. As an alternative approach, we performed VLCD treatment *in vitro* and assessed cleaved caspase 3, a marker of apoptosis. A dose-dependent increase in apoptotic marker cleaved caspase 3 was observed (Fig. 3), consistent with the *in vitro* and *in vivo* anti-tumor effect of VLCD we have observed in our previous studies [3].

Cerebellar Volumes on MicroCT-based VH Correlate Closely with MRI Cerebellar Volumes and Demonstrate Therapeutic Effects

Because MRI and microCT-based VH scans had different resolutions, the cerebellar volumes from each imaging modality varied slightly for the same mouse (Table 1). Perhaps related to volume-averaging effects or for formalin-associated tissue shrinkage, *in vivo* and *ex vivo* cerebellar volumes differed; however, a correlation plot of MRI versus microCT-based VH cerebellar volumes showed a strong correlation between the two datasets ($R=0.998$).

To assess a therapeutic effect of VLCD treatment, a two-way ANOVA test with a Bonferroni post-test was performed to compare the two methods in the two groups (Fig. 4a, b). The results indicated a significant difference between volumes of untreated cerebellums and treated cerebellums in both MRI (214.86 mm^3 vs. 113.30 mm^3 , $p=0.02$) and VH volume (144.55 mm^3 vs. 70.67 mm^3 , $p=0.04$) calculations.

Discussion

We have presented a rapid and inexpensive method of microCT-based VH method for imaging preclinical mouse models of medulloblastoma using treatment with VLCD as an example. VLCD is a first-in-class inhibitor of the 26S proteasome [8] and inhibition of the proteasome and protein recycling is a novel approach to treating cancers that was first demonstrated in multiple myeloma [8], although interest in other cancers is growing. In our study, microCT-based VH matched the tissue contrast achieved by more time- and cost-intensive MRI, while delivering more than tenfold-higher voxel diameter resolution.

To reduce the risk of anesthesia-associated death and to reduce the time and cost of scanning, the MRI scans for our study were non-isotropic with best resolution in the sagittal plane (Fig. 1). For better spatial resolution, MRI scans with isotropic resolution could be considered, but scan time and cost would increase accordingly. On the other hand, the *ex vivo* (post-mortem) method of microCT-based VH provided very good isotropic spatial resolution comparable to even an overnight post-mortem MRI scan. The data produced by the

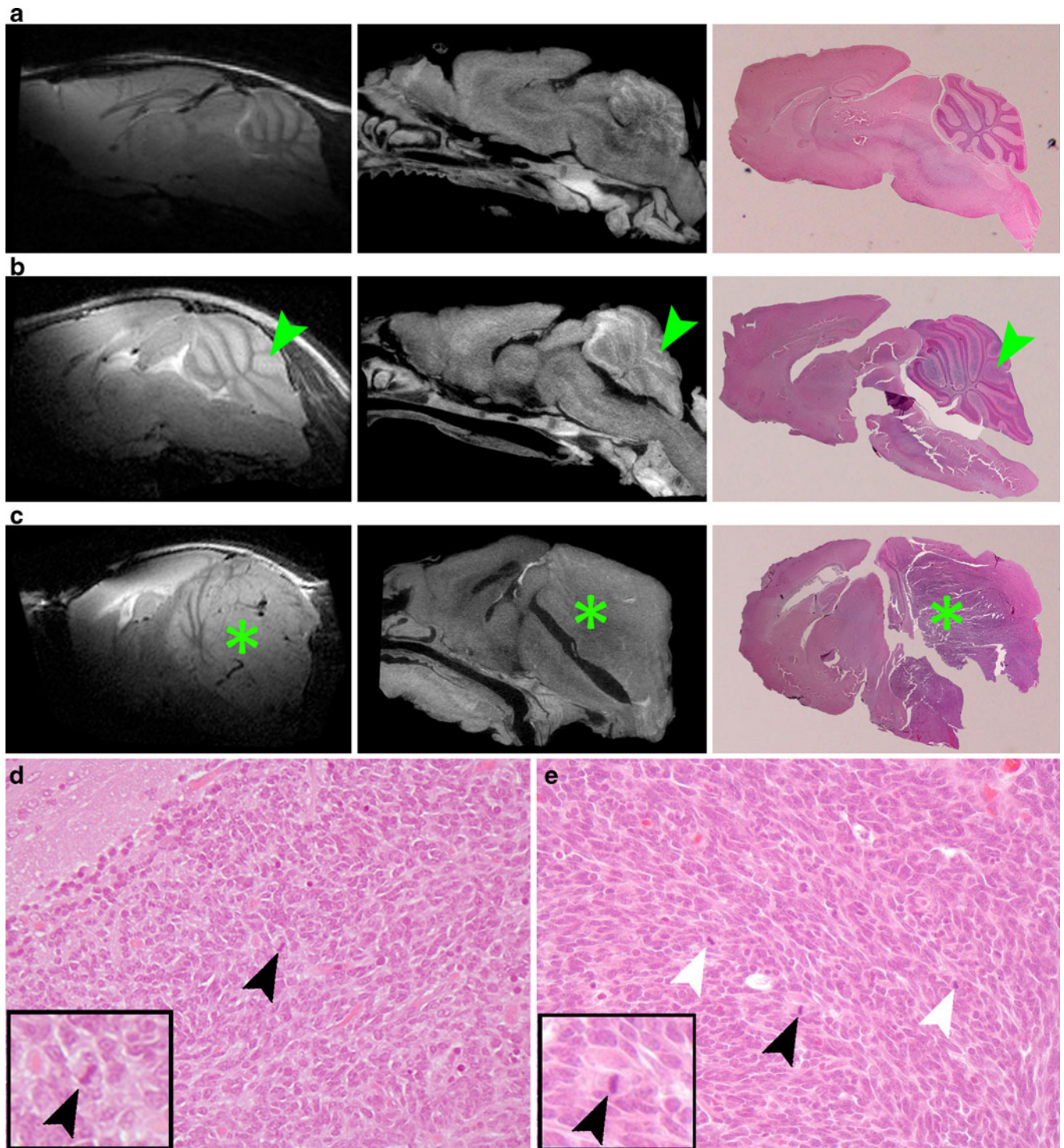


Fig. 2. Comparison between sagittal sections of MRI, microCT-based VH and histopathology images. MRI images (*left column*), microCT-based VH images (*middle column*) histopathology images (*right column*). **a** WT-DMSO mouse brain images for matching cross-sections. **b** MB-VLCD mouse brain images for matching cross-sections. Scan shows enlarged cerebellum with folia layer thickening, denoted by *arrowhead*. **c** MB-DMSO mouse brain images for matching cross-sections. *Asterisk* denotes tumor mass. **d, e** Histopathology MB-VLCD and MB-DMSO, respectively, are comparable, suggesting that residual (small) tumors may be protected by an intact blood-brain barrier. Mitotic count=4 and 31 per 10 HPF, respectively. *Insets* display zoom in view for the mitotic figure pointed by *black arrowheads*.

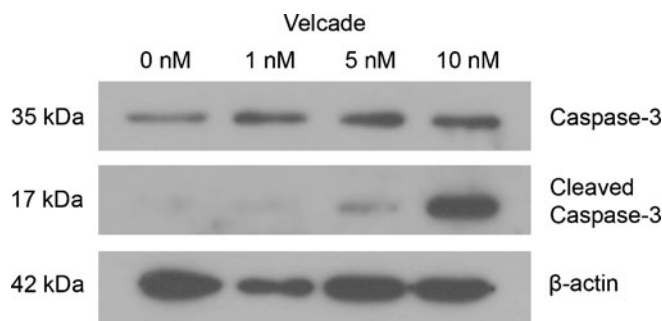


Fig. 3. The proteasome inhibitor VLCD results in a dose-dependent accumulation of cleaved Caspase-3 in medulloblastoma cell cultures *in vitro*. *Top and second row* Caspase-3 and pro-apoptotic Cleaved Caspase-3 following 0-, 1-, 5-, and 10-nM treatments with VLCD for 24 h. *Third row* β-actin, loading control. Western blots for each protein were taken at different exposures to optimize chemiluminescence.

microCT-based VH correlated well to histopathology, in part because of the ease with which isometric VH scan images can be adjusted to match any given plane (Fig. 2). Although fixation-associated tissue shrinkage occurred for samples, *ex vivo* cerebellar volumes on microCT-based VH correlated closely with MRI cerebellar volumes ($R=0.998$). Furthermore, microCT-based VH was equally effective at detecting therapy-related effects on primary medulloblastoma tumors for VLCD-treated mice (Fig. 4b), voxel volumes (resolution) was orders of magnitude better, and cost was more than 25% less. It is important to acknowledge, however, that MRI permits longitudinal assessment of intracranial tumor growth that may be important for preclinical studies different from ours, in which we only examined a single endpoint in our study.

For our analysis endpoints, we chose to measure cerebellar volume as a surrogate of tumor volume. This decision was based upon a pragmatic approach to what other academic and pharmaceutical investigators might pursue with most practicality (in the study of cerebellar tumors). We note, however, that for those interested in how treatment influences patterns of tumor invasion and effacement, the high-resolution anatomical information contained in microCT-based VH scans is more than adequate.

Finally, in a proof-of-concept experiment (Electronic Supplementary Material), we have determined that microCT-based VH is effective at detecting leptomeningeal

Table 1. Cerebellar volumes of non-treated and treated mice on MRI- and microCT-based VH techniques

MRI (volumes in mm ³)		microCT-based VH (volumes in mm ³)	
Non-treated (MB-DMSO)	Treated (MB-VLCD)	Non-treated (MB-DMSO)	Treated (MB-VLCD)
333.40	101.23	242.31	57.17
226.28	97.54	153	60.89
151.47	119.11	95.1	75.41
148.30	135.31	87.79	89.22

MB-DMSO medulloblastoma non-treated mice or treated with vehicle (DMSO), *MB-VLCD* medulloblastoma mice treated with VLCD

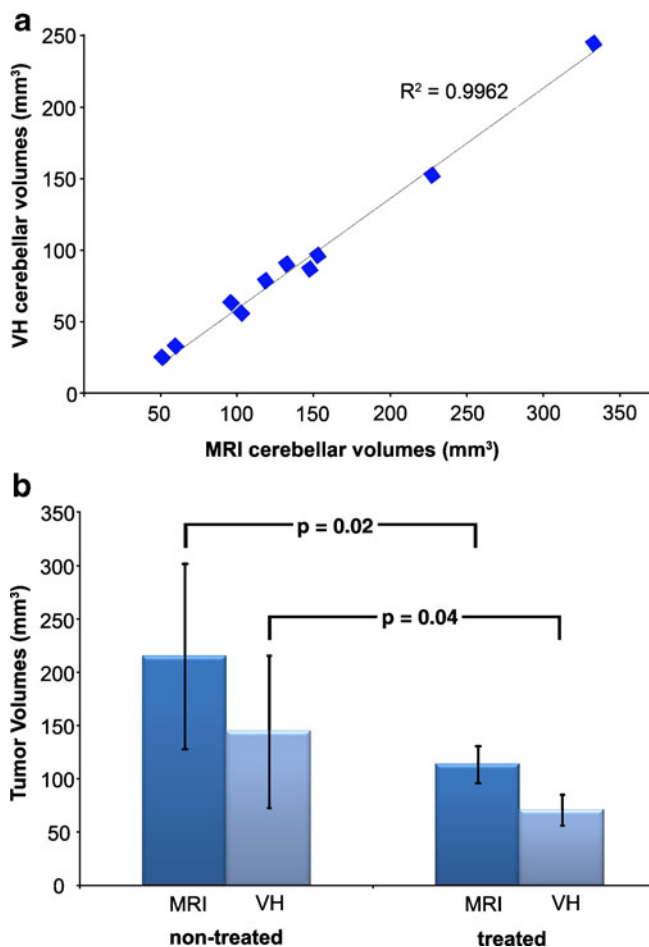


Fig. 4. Tumor volumes and therapeutic response. **a** Correlation between MRI and microCT-based VH tumor volumes. The x axis represents the cerebellar volumes (in mm³) from MRI images, y axis shows the corresponding cerebellar volumes (in mm³) from microCT-based VH images. **b** Statistical analysis for therapeutic response. The bar plots compare the non-treated and treated mice cerebellar volumes calculated from MRI and microCT-based VH images. The y axis shows the tumor volumes in mm³. The statistical difference between treated and non-treated group was significant ($p \leq 0.02$) and ($p \leq 0.04$) for MRI and microCT-based VH, respectively.

metastases, a condition difficult to detect with other imaging techniques of preclinical models (Electronic Supplementary Fig. 1) and painstaking if assessed by histopathology. At minimum, microCT-based VH would reduce significantly the time spent on histopathology by facilitating the rapid selection of areas of spine to section—and from which orientation.

In summary, microCT-based VH represents a versatile quantitative imaging method for anatomical imaging of the neuro-axis in preclinical models, particularly the next generation of GEMM. This imaging technique can be used as an adjunct or alternative to high-field MRI in therapeutic studies for measuring progression of brain tumors or leptomeningeal metastases.

Acknowledgments. C.K. is a member of the Cancer Therapy and Resource Center (2P30CA054174-17). This work was supported by a grant from the National Brain Tumor Society.

Disclosures. C.K. is co-founder of Numira Biosciences (www.numirabio.com), which licenses microCT-based virtual histology from UTHSCSA for commercial applications.

References

1. Koeller KK, Rushing EJ (2003) From the archives of the AFIP: medulloblastoma: a comprehensive review with radiologic-pathologic correlation. *Radiographics* 23:1613–1637
2. Roberts RO, Lynch CF, Jones MP, Hart MN (1991) Medulloblastoma: a population-based study of 532 cases. *J Neuropathol Exp Neurol* 50:134–144
3. Taniguchi E, Cho MJ, Arenkiel BR et al (2009) Bortezomib reverses a post-translational mechanism of tumorigenesis for patched1 haploinsufficiency in medulloblastoma. *Pediatr Blood Cancer* 53:136–144
4. Samano AK, Ohshima-Hosoyama S, Whitney TG et al (2009) Functional evaluation of therapeutic response for a mouse model of medulloblastoma. *Transgenic Res.* 2010 Jan 27.
5. Johnson JT, Hansen MS, Wu I et al (2006) Virtual histology of transgenic mouse embryos for high-throughput phenotyping. *PLoS Genet* 2:e61
6. Martinez HG, Prajapati SI, Estrada CA et al (2009) Images in cardiovascular medicine: microscopic computed tomography-based virtual histology for visualization and morphometry of atherosclerosis in diabetic apolipoprotein e mutant mice. *Circulation* 120:821–822
7. Palombella AL, Dutcher SK. (1998) Identification of the gene encoding the tryptophan synthase beta-subunit from *Chlamydomonas reinhardtii*. *Plant Physiol.* 1998 Jun;117(2):455–64
8. Hideshima T, Mitsiades C, Akiyama M et al (2003) Molecular mechanisms mediating antimyeloma activity of proteasome inhibitor PS-341. *Blood* 101(4):1530–1534